Double spin resonance in a spatially periodic magnetic field with zero average

A. Nogaret[1], F. Nasirpouri[1,7], J. -C. Portal[2,3,4], H. E. Beere[5], D. A. Ritchie[5], A. T. Hindmarch[6] and C. H. Marrows[6]

[1] *Department of Physics, University of Bath, Bath BA2 7AY, UK*
[2] *High Magnetic Field Laboratory, 25 Avenue des Martyrs, 38042 Grenoble, France*
[3] *Institut National des Sciences Appliquées, 31077 Toulouse, France*
[4] *Institut Universitaire de France*
[5] *Cavendish Laboratory, University of Cambridge, Cambridge CB3 0HE, UK*
[6] *School of Physics and Astronomy, University of Leeds, Leeds LS2 9JT, UK*
[7] *presently at: Department of Materials Engineering, Sahand University of Technology, Tabriz, Iran*

PACS 85.75.-d – Magnetoelectronics; spintronics: devices exploiting spin polarized transport or integrated magnetic fields
PACS 73.23.-b – Electronic transport in mesoscopic systems

Abstract –We report on the electrical detection of spin resonance in a two dimensional electron system modulated by a periodic magnetic field with zero average. Spin degeneracy is lifted by a large magnetic field applied in the plane while the system is irradiated with microwaves. Without magnetic modulation, the resistance does not detect spin resonance. However an absorption peak develops as the magnetic modulation is switched on. The frequency and temperature dependences of the peak yield the Zeeman energy of electrons in the GaAs/AlGaAs quantum well. We interpret the absorption peak as the result of competition between two spin flip transitions: one activated by snake orbits oscillating at the boundary between positive and negative magnetic field domains, the other by microwaves. When both transitions are simultaneously resonant, the system forms a dark state which blocks spin flips and freezes snake orbit channelling. The coherent suppression of snake orbit channelling explains the experimental features of the observed resonance.

Introduction. – The rapid emergence of spintronics is stimulated by the benefits of addressing individual spins in devices [1,2]. One way to control the spin is by shifting electrons between regions of opposite magnetic field. This can be done either by means of electrostatic gates [3] or by using the sign reversal of the Lorentz force to produce 'snake' orbits that meander between positive and negative magnetic field domains [4, 5]. Spatially varying magnetic fields which reverse sign are obtained by patterning ferromagnets at the surface of a two-dimensional electron gas (2DEG). The undulation of snake trajectories in the canted magnetic field subjects the electron spin to a time dependent magnetic field that oscillates at microwave frequencies ∼100GHz. Snake induced Electron Spin Resonance (SESR) occurs when the oscillation frequency of a snake orbit equals $g\mu_B B_0/\hbar$ [6]. A feature that has received little attention is the huge amplitude of the alternating magnetic field, typically ∼0.1T, which makes the Rabi frequency larger than the spin relaxation rate and opens the possibility of coherently manipulating the electron spin.

Here, we investigate the electrical conductivity of lateral magnetic superlattices under microwave irradiation to study the interplay between SESR and Microwave induced Electron Spin Resonance (MESR). The grating applies a spatially varying magnetic field that deflects electron trajectories in the two dimensional electron gas (2DEG). An external magnetic field is applied in the plane to induce spin precession. We report an absorption peak in the resistance of the magnetically modulated 2DEG when MESR crosses resonance. Such peak is a priori unexpected because, the density of states being two-dimensional, spin up and spin down channels have equal conductivities. In which case, spin flips would leave the resistance unchanged. We verify that this assumption is true in the unmodulated 2DEG. By switching the magnetic modu-

lation off we have demonstrated the suppression of the resistance peak. Our experiment differs from earlier experiments on resistively detected spin resonance in that here the 2DEG is ballistic and Landau quantization is not used to differentiate spin up and spin down conductivities [7–9]. We measure the frequency dependence of the absorption peak and obtain the Landé g-factor of electrons in the GaAs/AlGaAs heterojunction. We also find that the thermal activation energy of the absorption peak corresponds to the Zeeman energy in the GaAs quantum well. To explain the change in resistance caused by spin flips, we argue that inhomogeneous magnetic fields introduce electron states that couple orbital and spin motion. One example of these states are snake orbits whose spin phase depends on the electron path in the magnetic potential. Here, we show that the MESR transition freezes snake orbit channelling by blocking spin flips. We compute the change in resistance induced by the SESR and MESR transitions and use the resulting equation to fit the experimental peak. The fit gives the spin relaxation rate and the Rabi frequency of the MESR transition as adjustment parameters.

Experimental. – Cobalt finger gates were fabricated at the surface of the GaAs/$Al_{0.33}Ga_{0.67}As$ single heterojunction pictured in Fig.1(a). We used Hall devices with longitudinal finger gates to measure the magneto-resistance and the Hall resistance. The electron mobility, $\mu = 1.5 \times 10^6 \mathrm{cm}^2.\mathrm{V}^{-1}.\mathrm{s}^{-1}$, and density, n_s=1.6±0.1×$10^{11}\mathrm{cm}^{-2}$ ($k_F = \sqrt{2\pi n_s}$), were determined by quantum transport in a perpendicular magnetic field. The magnetic structure of the cobalt grating was imaged by magnetic force microscopy - see Fig.1(b). When the grating is magnetized along y, magnetic poles form at the edges of the stripes (dark lines). The poles vanish when the magnetization is parallel to x.

Magnetic poles generate a fringing magnetic field at the site of the 2DEG. This field has two vector components $B_{1,z}(y) = \tilde{B}_1 \sin(Qy)$ and $B_{1,y}(y) = \tilde{B}_1 \cos(Qy)$ where $Q = 2\pi/a$. Higher harmonics exist but are negligible given the large separation between the grating and the 2DEG ($\pi[z_0 + w/2] > a$) [10, 11]. The magnetic potential forms snake orbits at sites $y_n = na/2$ ($n = 0, \pm 1...$) where $B_{1,z}$ cancels [12]. Snake orbits are demonstrated through their giant magnetoresistance in a perpendicular magnetic field which in the case of our grating is $\Delta\rho_{yy}/\rho_0 \approx 1800\%$ [13].

Experiments were conducted in an external magnetic field B_a applied in the plane of the 2DEG. B_a was used to magnetize the cobalt fingers. We were able to turn the magnetic potential ON or OFF by applying B_a along the short or the long axis of the stripes. B_a was also used as the Larmor field giving the frequency of spin precession $\omega_0 = g_\parallel \mu_B B_0/\hbar$. B_a was carefully aligned with the 2DEG to minimize any residual perpendicular component. The sample was first coarsely aligned on the probe to within 1°. The in-plane alignment was then finely tuned by adjusting the height of the sample relative to the center of the

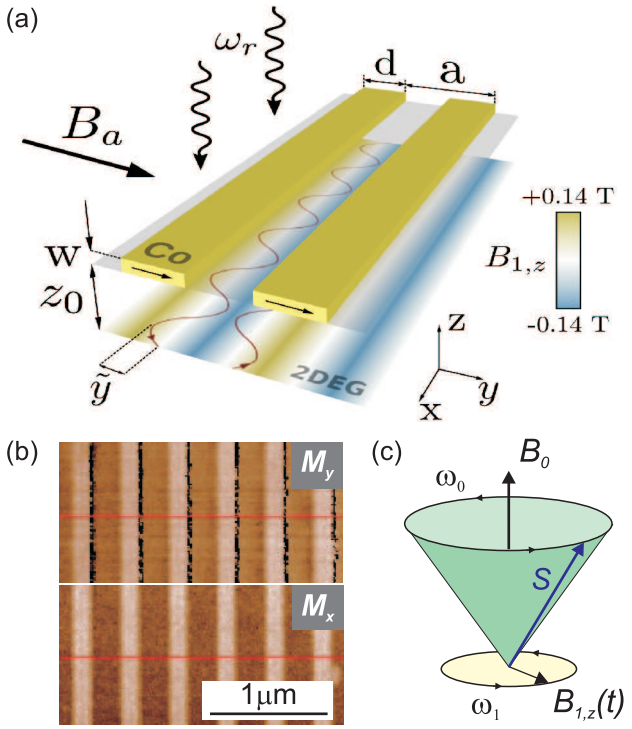

Fig. 1: (a) Magnetic superlattice: the cobalt grating modulates the 2DEG with a sinusoidal magnetic field $B_{1,z}(y)$ which bends ballistic trajectories in snake orbits (red lines), the superlattice is irradiated with microwaves at frequency ω_r and is subjected to a homogeneous magnetic field B_a; (b) MFM images of the Co grating magnetized along y (top) and along x (bottom); (c) SESR occurs when the oscillation frequency of snake orbits ω_1 equals the spin precession frequency ω_0 ($B_0 = B_a + B_N$). MESR is the spin resonance of microwaves at $\omega_r = \omega_0$. Parameters: $a = 400nm$, $d = 200nm$, $w = 160nm$ and $z_0 = 90nm$.

superconducting magnet. The Hall resistance minimum was found within ±2cm of the centre of the field. Samples were mounted vertically at the end of an overmoded circular waveguide. A copper mirror was used to redirect microwaves onto the sample surface as shown in Fig.1(a). The resistance was measured using low frequency lock in detection, the current bias (500nA) was along the stripes (x-direction).

The low field magnetoresistance ρ_{xx} and the Hall resistance ρ_{xy} are now used to obtain the amplitude of the magnetic modulation $\tilde{B}_1$. The dependence of ρ_{xx} on $B_a \parallel y$ (full lines) and $B_a \parallel x$ (dashed lines) is shown in Fig.2(a). When $B_a \parallel y$, a V-shaped magnetoresistance of magnitude $\Delta\rho_{xx}/\rho_0 = 25\%$ develops between 0 and ±0.30T. This range of magnetic fields corresponds to the reversal of the magnetization in the Co grating [Fig.2(b)]. $\Delta\rho_{xx}/\rho_0$ hence results from the reduction of the electron mean free path by the rising magnetic modulation. The sinusoidal magnetic field $B_{1,z}(y)$ decreases the number of ballistic conduction channels [12] by introducing magnetic poten-

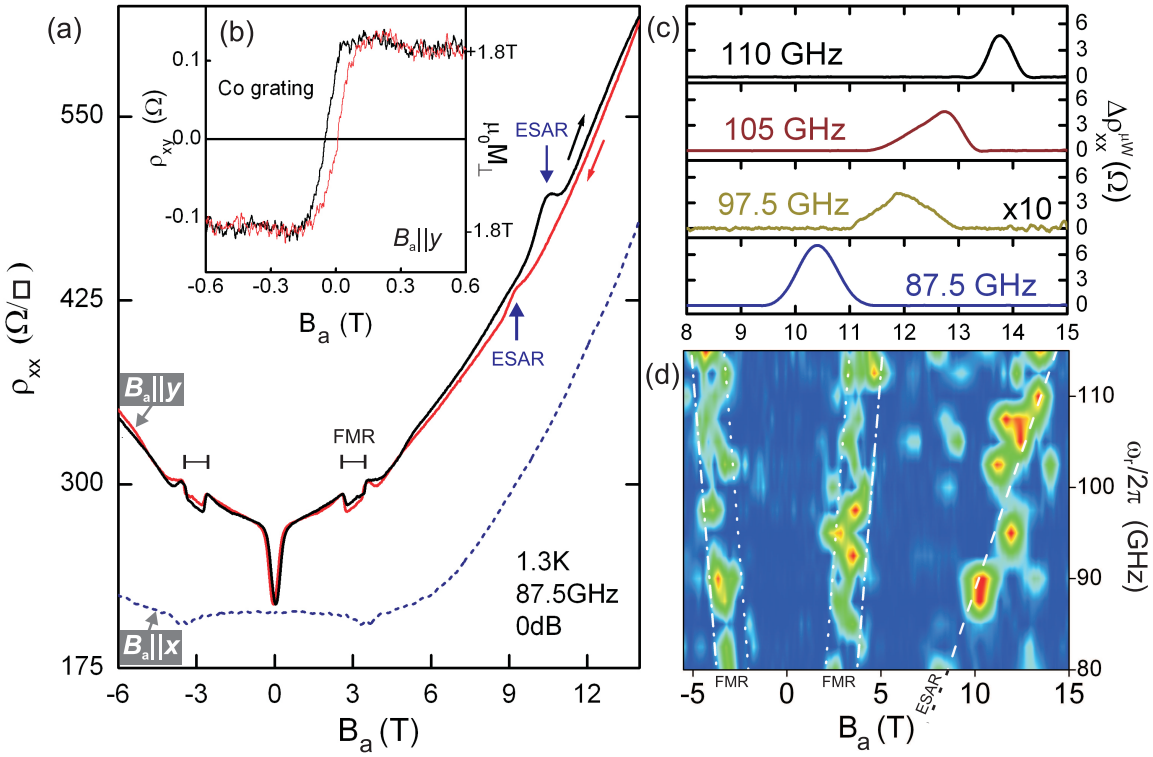

Fig. 2: (a) Magnetoresistance of the cobalt superlattice measured with $B_a \parallel y$ (full lines) and $B_a \parallel x$ (dotted lines); (b) magnetization curve of the cobalt grating measured by Hall magnetometry ($B_a \parallel y$); (c) frequency dependence of the ESAR peak; (d) microwave induced resistance $\Delta\rho_{xx}^{\mu W}$ mapped as a function of ω_r and B_a ($B_a \| y$).

tial barriers [11,14] which reflect electrons with transverse momentum $k_y < k_b = e\tilde{B}_1 a/h$. Such modes are confined to one period of the magnetic superlattice. Modes with momentum $k_y > k_b$ extend over the barriers, over approximately 30 lattice periods, a distance limited by the mean free path. A simple calculation shows that the magnetic potential decreases the number of extended modes by $\Delta N/N_0 = (1-k_b/k_F)^2 - 1$. As a result, the Drude resistivity $\rho_0 = (h/e^2)N_0^{-1}$ increases by $\Delta\rho_{xx}/\rho_0 = -\Delta N/N_0$. Given that $\Delta\rho_{xx}/\rho_0 = 25\%$, we estimate the amplitude of the magnetic modulation to be $\tilde{B}_1$ =0.139T. A calculation of the field emanating from the grating [10, 11] gives $\tilde{B}_1 = \mu_0 M_y/(2\pi)\sin(Qd/2)\sinh(Qw/2)e^{-Q(z_0+w/2)}$. Using the tabulated saturation magnetization of Cobalt $\mu_0 M_y$ =1.82T and the device dimensions in Fig.1(a), we find $\tilde{B}_1$ =0.141T, in agreement with the experimental value. When $B_a \parallel x$, the V-shaped magnetoresistance vanishes, not surprisingly, because $M_y = 0$ gives $\tilde{B}_1 = 0$.

We now turn to the microwave induced structure in Fig.2(a). We label the resistance peak at 10.3T ESAR (Electron Spin Anti-Resonance) because conventional ESR is not detected in the ballistic regime of the 2DEG. The conductivities of spin up and spin down electrons being the same, spin flips have no net effect on the overall conductivity. We verify this by magnetizing the stripes along x to suppress the magnetic modulation (dotted lines) and show that the resistance has no absorption peak at any value of the microwave power. The magnetic potential must therefore introduce electron states that couple the spin to the orbital dynamics enabling the electrical detection of spin resonance. At low magnetic field, the 2DEG detects the ferromagnetic resonance (FMR) of the grating giving the dip seen between 2.6T and 3.5T (full lines).

The ESAR and FMR are identified by their frequency dependence in Figs.2 (c) and (d). Panel (d) maps the ESAR and FMR amplitude $|\Delta\rho_{xx}^{\mu W}|$ obtained by subtracting the background resistance measured at zero microwave power. The frequency dependence of the ESAR peak position was interpolated with a least square method weighting in the peak amplitudes (dashed line) which we fitted using the frequency dependence of the Zeeman gap $\omega_r = |g_\parallel|\mu_B(B_a + B_N)/\hbar$. ω_r is the angular frequency of microwaves, μ_B is the Bohr magneton and $g_\parallel$ is the Landé g-factor in the quantum well. The fit gives $|g_\parallel|$=0.43±0.04 and B_N=4.53T±0.3T. The Landé factor obtained from a fit of FMR is g^*=1.8±0.04. The accepted value for Cobalt is $g^* = 1.83$ [15].

The Landé g-factor in the quantum well can also be obtained from the temperature dependence of the ESAR peak - see Fig.3 (b). The amplitude of the ESAR peak $\Delta\rho_{xx}^{\mu W}(T)$ is assumed to be proportional to the fraction of redistributed spins $(N_\uparrow - N_\downarrow)/N_\uparrow = 1 - \exp(-\Delta/k_B T)$ where Δ is the Zeeman gap. Hence,

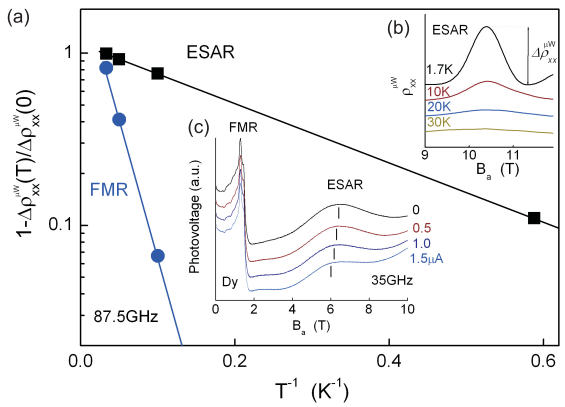

Fig. 3: (a) Thermal activation of ESAR and FMR peak amplitudes; (b) Temperature dependence of the ESAR peak; (c) Current dependence of the ESAR peak in a dysprosium superlattice.

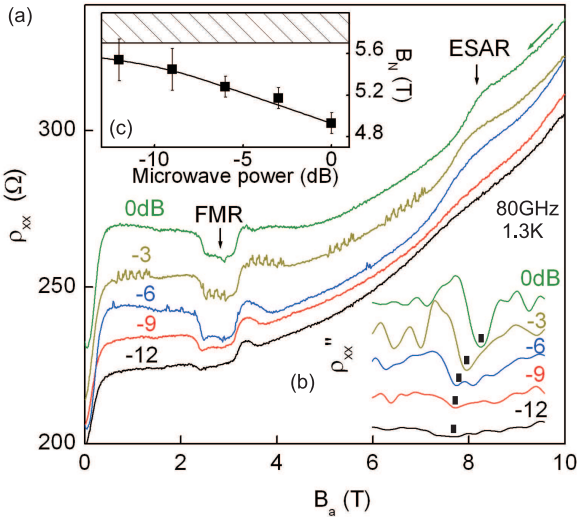

Fig. 4: (a) Dependence of ρ_{xx} on microwave power; (b) second derivative of the resistance curves near the ESAR peak; (c) Dependence of B_N on microwave power.

the peak amplitude follows the thermal activation law $\Delta\rho_{xx}^{\mu W}(T) = \Delta\rho_{xx}^{\mu W}(0)\{1-\exp[-\Delta/(k_BT)]\}$. The ratio $\Delta\rho_{xx}^{\mu W}(1.7K)/\Delta\rho_{xx}^{\mu W}(0) = 0.89$ was obtained by requiring the alignment of the data points in Fig.3(a). The slope gave the activation energy: $\Delta = 0.342$meV. Writing $\Delta = |g_\parallel|\mu_B(B_a + B_N)$, $B_a = 10.3$T and $B_N = 4.53$T, the fit of the temperature dependence gives $|g_\parallel| = 0.40$. Within experimental error, this is the g-factor obtained from the frequency dependence. The theoretical value for a 15nm wide GaAs quantum well [16] is $g_\parallel = -0.42$.

The dependence of the ESAR peak on microwave power is obtained in Fig.4. B_N is obtained from the shift of the peak position relative to the bare resonant field given by $\hbar\omega_r/(g\mu_B)$. Panel (c) shows that B_N decreases from 5.6T at -12dB to 4.9T at 0dB and that it extrapolates to 5.7 ± 0.2T at zero microwave power. This a priori suggests that the nuclear spin system is polarized close to saturation [17] at zero microwave power. To determine whether SESR might dynamically polarize nuclear spins, we study the dependence of B_N on the intensity of the current drive. This study was done in a dysprosium superlattice and is shown in Fig.3(c). The ESAR peak shifts to lower field when the current increases which shows that B_N increases from 0T at 0μA to 0.45T at 1.5μA. In the meantime the position of the FMR peak is constant which eliminates heating as the source of the drift. The increase in B_N with increasing current suggests that the current dynamically polarizes nuclei possibly through the SESR mechanism. By contrast, increasing the microwave power reduces B_N. The joint effect of MESR and SESR is to decrease the nuclear spin polarization. One may also assume that the hysteresis of the ESAR peak is due to the long relaxation time of nuclei after these have been dynamically polarized when the electron system crosses the antiresonance.

Snake oscillators in a sinusoidal magnetic field. – We develop a semiclassical theory of snake orbits in a sinusoidal magnetic field to calculate both the angular frequency of snake oscillations ω_1 and the Rabi frequency of the SESR transition Ω_1. The inhomogeneous magnetic field deflects the electron velocity at a rate $(\dot v_x, \dot v_y) = \omega_c(y)(-v_y, v_x)$ where $\omega_c = eB_{1,z}(y)/m^*$ is the local cyclotron frequency in the magnetic field $B_{1,z}(y) = \tilde B_1 \sin(Qy)$ ($\tilde B_1 = 0.141$T). $v_x(y)$ is easily obtained by integration once the initial condition $v_x(y=0) = v_F\cos\theta$ is specified. θ is the angle at which the trajectory crosses the line of zero magnetic field. $v_y(y)$ is obtained by stating that the total electron velocity is the Fermi velocity: $v_x^2 + v_y^2 = v_F^2$. One arrives at the transverse equation of motion of the snake oscillator:

$$(\tau\dot Y)^2 = [1-\gamma^2Y^2][\cos^2(\theta/2) - Y^2][Y^2 + \sin^2(\theta/2)]. \quad (1)$$

The position Y is dimensionless and relates to the real space coordinate y through:

$$Y = \sin(Qy/2)/\gamma, \quad (2)$$

where $\gamma = Ql$ (2.7) and $l = \sqrt{\hbar k_F/(eb)}$ (172nm) is the largest possible amplitude of an oscillator [6] in gradient of magnetic field b. In the case of a sinusoidal magnetic modulation $b = Q\tilde B_1$ (2.2T/μm). Eq.1 describes an anharmonic oscillator centered at $y = 0$ and oscillating with amplitude $\tilde Y = \cos(\theta/2)$. The amplitude of oscillations in real space $\tilde y$ depends on the strength of the magnetic confinement through parameter γ. If $\gamma < 1$ (strong magnetic confinement), Eq.1 has real solutions because its right hand side is always positive. The maximum possible value for $\tilde Y$ is 1 as a result all electrons on the Fermi surface are confined to a bundle of snake orbits of width $\tilde y_{max} = (2/Q)\arcsin\gamma$. If $\gamma > 1$ (weak magnetic confinement), there exists a critical angle θ_c at which a snake orbit touches the boundary of the superlattice period ($\tilde y = a/2$)

and becomes an extended orbit. Setting $\tilde{y} = a/2$ in Eq.2 gives $\tilde{Y} = \gamma^{-1}$, hence $\theta_c = 2\arccos(\gamma^{-1})$. With $\gamma = 2.7$, our superlattice falls into this second category with a critical angle $\theta_c = 136°$. Trajectories with angle θ comprised between 180° and 136° are snake orbits. Those between 136° and 0 are extended orbits.

The period of the oscillator is calculated by integrating Eq.1. The angular frequency of snake oscillations is $\omega_1(\tilde{y}) = \tilde{\omega}_1/[4F(\pi/2, \tilde{y})]$ where:

$$F\left(\frac{\pi}{2}, \tilde{y}\right) = \int_0^{\pi/2} \frac{d\alpha}{\sqrt{1 - \tilde{Y}^2\left[1 + \gamma^2(1 - \tilde{Y}^2)\right]\sin^2\alpha}}. \quad (3)$$

$\tilde{\omega}_1 = \sqrt{\hbar k_F e b}/m^*$ is the maximum angular frequency of snake oscillators and $\tilde{Y} = \sin(Q\tilde{y}/2)/\gamma$. We parametrize ω_1 with $\tilde{y}$ rather than θ to facilitate the discussion given that $\tilde{y}$ varies between 0 and $a/2$. $\tilde{y}$ is related to θ through the relation $\gamma\cos(\theta/2) = \sin(Q\tilde{y}/2)$. The dispersion curve $\omega_1(\tilde{y})$ is plotted in Fig.5(a). Snake orbits of amplitude $\tilde{y} \sim 0$ oscillate at the maximum frequency $\tilde{\omega}_1/(2\pi)$ =150GHz whereas those of maximum amplitude $\tilde{y} \sim a/2$ have zero frequency. The Rabi frequency of SESR is $\Omega_1(\tilde{y}) = |g_\parallel|\mu_B B_{1,z}(\tilde{y})/\hbar$ and is plotted in Fig.5(b). $\Omega_1(\tilde{y})$ has a maximum $\tilde{\Omega}_1/(2\pi) = 0.81$GHz at $\tilde{y} = a/4$.

The SESR picture is summarized in Fig.1(c). Resonance is reached at $\omega_1 = \omega_0$. When this happens, the wiggling motion of a snake orbit is accompanied by spin flips. The rate of spin flips (Rabi frequency) is about 100 times slower than the frequency of the snake oscillator. The standard textbook picture of MESR requires the three following modifications to properly describe SESR: the alternating magnetic field of SESR is linearly polarized instead of being circularly polarized, it is periodic but not sinusoidal [6], spin flips are propelled by the electric bias not by photons as in MESR. In MESR, Rabi oscillations involve the absorption and re-emission of the same photon. In SESR, a spin gains energy by absorbing a small fraction of the kinetic energy of an electron accelerated in the d.c. electric field. This energy is then given back to the electron when the spin returns to its ground state in the second half of the cycle.

Double spin resonance. – The Zeeman gap is bridged by *two* transitions which couple states $|\downarrow, N>$, $|\downarrow, N+1>$ and $|\uparrow, N>$ - see Fig.5(c). Here N is the number of microwave photons in the sample cavity at frequency ω_r. The SESR transition (ω_1,Ω_1) conserves the photon number whereas the MESR transition (ω_r,Ω_r) does not. The SESR transition remains resonant because the oscillator spectrum is continuous. There is always one oscillator mode matching the Larmor frequency so that the resonant condition $\omega_1 = \omega_0$ is satisfied. When the microwave transition crosses resonance at $\omega_r = \omega_0$, the initial states hybridize to form a dark state: $|d> = \frac{\Omega_1}{\sqrt{\Omega_1^2+\Omega_r^2}}|\downarrow, N+1> - \frac{\Omega_r}{\sqrt{\Omega_1^2+\Omega_r^2}}|\downarrow, N>$. The system decays into this state with no way out since $|d>$ has no component on $|\uparrow, N>$. The probability of the dark state is the expectation value of the density matrix:

$$P_{dark} = < d|\hat{\rho}|d > \quad (4)$$

One obtains the density matrix given the hamiltonian of the unperturbed three level system $\hat{H}_0 = \hbar\omega_0|\downarrow, N>$, and the interaction hamiltonian arising from both transitions:

$$H_{int} = -\frac{\hbar}{2}\begin{pmatrix} 0 & 0 & \Omega_r \\ 0 & 2\delta & \Omega_1 \\ \Omega_r & \Omega_1 & -2\delta \end{pmatrix} \quad (5)$$

where $\delta = \omega_0 - \omega_r$ is the detuning of microwaves from resonance. The density matrix obeys the following rate equations [18]:

$$\dot{\rho}_{11} = \frac{i}{2}\Omega_r(\rho_{31} - \rho_{13}) + \rho_{33}\frac{\gamma_T}{2}, \quad (6)$$

$$\dot{\rho}_{22} = \frac{i}{2}\Omega_1(\rho_{32} - \rho_{23}) + \rho_{33}\frac{\gamma_L}{2}, \quad (7)$$

$$\dot{\rho}_{33} = \frac{i}{2}\left[\Omega_r(\rho_{13} - \rho_{31}) + \Omega_1(\rho_{23} - \rho_{32})\right] - \rho_{33}\gamma_L, \quad (8)$$

$$\dot{\rho}_{12} = \frac{i}{2}\left[\Omega_r\rho_{32} - \Omega_1\rho_{13}\right] + \rho_{12}(i\delta - \frac{\gamma_T}{2}), \quad (9)$$

$$\dot{\rho}_{13} = \frac{i}{2}\left[\Omega_r(\rho_{33} - \rho_{11}) - \Omega_1\rho_{12}\right] + \rho_{13}(i\delta - \frac{\gamma_L}{2}), \quad (10)$$

$$\dot{\rho}_{23} = \frac{i}{2}\left[\Omega_1(\rho_{33} - \rho_{22}) - \Omega_r\rho_{21}\right] - \rho_{23}\frac{\gamma_L}{2}, \quad (11)$$

where γ_T and γ_L are the transverse and longitudinal spin relaxation rates and $|1> \equiv |\downarrow, N+1>$, $|2> \equiv |\downarrow, N>$ and $|3> \equiv |\uparrow, N>$. One solves the system, seeking time independent solutions, by successive approximations to second order in Ω_r/Ω_1. Taking $\rho_{11} \approx 1$, $\rho_{22} \approx 0$, $\rho_{33} \approx 0$ as initial conditions and assuming that $\gamma_L \cong \gamma_T$ for conduction electrons, one obtains:

$$P_{dark} = \frac{4\Omega_1^2\Omega_r^2}{\Omega_1^2 + \Omega_r^2}\frac{\Omega_1^2 + \gamma_L\gamma_T}{(\Omega_1^2 + \gamma_L\gamma_T - 4\delta^2)^2 + 4\delta^2(\gamma_L + \gamma_T)^2}. \quad (12)$$

The resonant snake orbits are accompanied by spin flips. Blocking their propagation stops spin flips. Conversely if spin flip is not allowed, the Zeeman gap acts as an energy barrier to the propagation of snake orbits - as shown by the temperature dependence in Fig.3. We obtain the microwave induced resistance by writing the sample conductivity as a sum of two components. One component is the conductivity along the path of snake orbits $\sigma_s(1 - P_{dark})$. The other component Σ incorporates the conductivity of all other orbits which are not bound by the magnetic potential. The conductivity in the absence of microwaves is $\sigma_0 = \sigma_s + \Sigma$. The change in longitudinal resistance brought by the formation of the dark state then writes:

$$\frac{\Delta\rho_{xx}^{\mu W}}{\rho_0} = \rho_0\sigma_s P_{dark}. \quad (13)$$

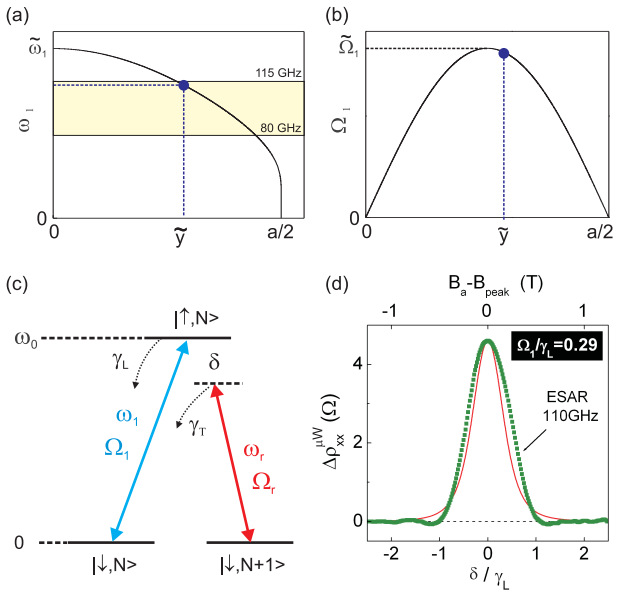

Fig. 5: (a) Frequency spectrum of snake oscillators and (b) their Rabi frequency plotted as a function of the oscillator amplitude; (c) SESR driven transition (ω_1, Ω_1) and MESR transition (ω_r, Ω_r) across the Zeeman gap. There are N photons in mode ω_r, the longitudinal and transverse spin relaxation rates are γ_L and γ_T. (d) Fit of the ESAR line at 110GHz (squares) with Eq.13 (full lines).

Eq.13 shows that the amplitude of the resistance peak is proportional to the probability of the dark state. The dark state increases the resistance by blocking spin flips and freezing snake orbit drift. We estimate $\rho_0\sigma_s \approx 1800\% \pm 360\%$ from the change in resistance caused by suppression of snake orbit channelling [13].

Eqs.12 and 13 describe the ESAR peak that results from the coherent interaction of MESR and SESR. We now use these equations to fit the ESAR peak in Fig.5(d). The Rabi frequency that corresponds to a microwave frequency of 110GHz is obtained as follows. Setting 110GHz on the vertical axis of Fig.5(a) gives $\tilde{y} \approx a/4$ on the horizontal axis. Reporting this value on the horizontal axis of Fig.5(b) gives a Rabi frequency close to the theoretical maximum. Using the calculated value $\tilde{\Omega}_1/(2\pi) = 0.81$GHz, we find that Eq.13 fits the width of the peak best for spin scattering rates $\gamma_L = \gamma_T = 1.76 \times 10^{10} s^{-1}$. This spin scattering rate is close to the momentum scattering rate $\mu m^*/e = 1.4 \times 10^{10} s^{-1}$ which suggests that the spin relaxation time is limited by the lifetime of snake orbits. One also notes that $\tilde{\Omega}_1 = 0.29\gamma_L$ which indicates that there is sufficient time for spins to flip between two scattering events. This fulfills the condition of quantum coherence required for the formation of the dark state. The fit of the ESAR peak amplitude with Eq.13 gives an estimate of the Rabi frequency Ω_r of the MESR transition. The accuracy of the fit is limited by the accuracy on $\rho_0\sigma_s$ and gives $\Omega_r/(2\pi) = 70 \pm 15$MHz. The fact that $\Omega_r \ll \Omega_1$ can be verified by examining the dependence of the ESAR peak amplitude on microwave power - see Fig.4(b). In this case, Eq.12 predicts that $P_{dark} \propto \Omega_r^2 \propto \tilde{B}_r^2$, meaning that the probability of the dark state increases linearly with microwave power. In the opposite case $\Omega_r \gg \Omega_1$, P_{dark} would have been independent of the microwave power.

In summary, magnetic superlattices allow the electrical detection of spin resonance by forming orbits that couple orbital and spin motion. We interpret the resistance peak as the result of the coherent interaction between SESR and MESR which decreases the conductivity of snake states. Spatially varying magnetic fields reveal to be an attractive system for coherent spin manipulation.

* * *

We acknowledge financial support from the EPSRC(UK), the EU transnational access to High Magnetic fields RITA-CT-2003-505474 and the technological contribution of B.Dai and P.Saraiva.

REFERENCES

[1] Hanson R. and Awschalom D. D., *Nature*, **453** (2008) 1043.
[2] Hanson R., Kouwenhoven L. P., Petta J. R., Tarucha S. and Vandersypen L. M. K., *Rev. Mod. Phys.*, **453** (2008) 1043.
[3] Pioro-Ladrière M., Obata T., Tokura Y., Shin Y. -S., Kubo T., Yoshida K., Taniyama T. and Tarucha S., *Nature Phys.*, **4** (2008) 776.
[4] Ye P. D., Weiss D., Gerhardts R. R., Seeger M., von Klitzing K., Eberl K. and Nickel H., *Phys. Rev. Lett.*, **74** (1995) 3013.
[5] Nogaret A., Bending S. J. and Henini M., *Phys. Rev. Lett.*, **84** (2000) 2231.
[6] Nogaret A., *Phys. Rev. Lett.*, **94** (2005) 147207.
[7] Stein D., von Klitzing K. and Weiman G., *Phys. Rev. Lett.*, **51** (1983) 130.
[8] Dobers M., von Klitzing K. and Weiman G., *Phys. Rev. Lett.*, **38** (1988) 5453.
[9] Jiang H. W. and Yablonovitch E., *Phys. Rev. B*, **64** (2001) 041307.
[10] Gerhardts, R. R., *Phys. Rev. B*, **53** (1996) 11064.
[11] Ibrahim I. S. and Peeters F. M., *Phys. Rev. B*, **52** (1995) 17321.
[12] Reijniers J. and Peeters F. M., *Phys. Rev. B*, **63** (2001) 165317.
[13] Nogaret A., Overend N., Gallagher B. L., Main P. C., Henini M., Marrows C. H., Howson M. A. and Beaumont S. P., *Physica E*, **2** (1998) 421.
[14] Oakeshott R. B. S. and MacKinnon A., *J. Phys. Cond. Mat.*, **5** (1993) 9355.
[15] Scott, G. G., *Phys. Rev.*, **104** (1956) 1497.
[16] Kiselev, A. A. and Ivchenko, E. L. and Rössler, U., *Phys. Rev. B*, **58** (1998) 16353.
[17] Paget D., Lampel G., Sapoval B. and Safarov V. I., *Phys. Rev. B*, **15** (1977) 5780.
[18] Fleischhauer M., Imamoglu A. and Marangos J. P., *Rev. Mod. Phys.*, **77** (2005) 633.